Hindawi Publishing Corporation
Shock and Vibration
Volume 2014, Article ID 801696, 11 pages
http://dx.doi.org/10.1155/2014/801696

Research Article

Free Vibration Behavior of a Gradient Elastic Beam with Varying Cross Section

Mustafa Özgür Yayli

Department of Civil Engineering, Faculty of Engineering, Bilecik Şeyh Edebali University Gülümbe Kampüsü, 11210 Bilecik, Turkey

Correspondence should be addressed to Mustafa Özgür Yayli; mozgur.yayli@bilecik.edu.tr

Received 12 July 2013; Accepted 3 December 2013; Published 17 February 2014

Academic Editor: Nuno Maia

Based on strain gradient elasticity theory, a finite element procedure is proposed for computation of natural frequencies for the microbeams of constant width and linear varying depth. Weak form formulation of the equation of motion is obtained first as in common classical finite element procedure in terms of various kinds of boundary conditions. Gradient elastic shape functions are used for interpolating deflection inside a finite element. Stiffness and mass matrices are then calculated to solve the microbeam eigen value problem. A solution for natural frequencies is obtained using characteristic equation of microbeam in gradient elasticity. The results are given in a series of figures and compared with their classical counterparts. The effect of various slope values on the natural frequencies are examined in some numerical examples. Comparison with the classical elasticity theory is also performed to verify the present study.

1. Introduction

Microbeams have held wide applications in micro-electronic-mechanical systems (MEMS) such as those in actuators [1], microswitches [2], microresonators [3], Atomic Force Microscopes [4], and sensors [5] in which thicknesses and lengths of microbeams are typical on the order of microns and submicrons; therefore the small scale effects in their static and dynamic behavior are considerable.

In the past decades, some researchers have tried to establish experimental and theoretical models for vibration of microbeams. However, most of these studies are based on the classical continuum mechanics. The classical model is doubtful whether it can describe the static or dynamic behaviour of elastic materials with microstructure, since it is associated with the concepts of locality of the stress. The experimental studies have also revealed that the classical continuum mechanics is unable to consider size-dependent static and dynamic behaviours in microscaled structures [6, 7]. Lam et al. [8] observed experimentally that the normalized bending stiffness increases by about 2.4 times when the thickness was reduced from 115 to 20 μm; Stolken and Evans [9] examined that the plastic work hardening shows a great increase as the microbeam thickness decreases from 50 to 12.5 μm. These results demonstrate that the size dependence is significant to certain materials.

During past years, some nonclassical elasticity theories such as the strain gradient, nonlocal, and couple stress theories have been introduced and employed to investigate the microbeams. Nonclassical continuum theories can be classified to couple stress and strain gradient approaches. The couple stress theory includes higher-order stresses, known as the couple stresses. The classical couple stress theory was originated by Mindlin [10] and others including Toupin [11] in 1960s. Some related research works have been performed to model the static and dynamic problems based on the classical couple stress theory [12, 13]. A new modification to couple stress theory has been proposed by Mindlin [14] in which a new equilibrium equation of high order is considered in addition to the classical equilibrium equations of forces and moments of forces. So far Park and Gao [15] have developed the static bending; Kong et al. [16] have developed free vibration problems of a Euler-Bernoulli beam. Ma et al. [17] have developed the static bending and free vibration problems of a Timoshenko beam. dos Santos and Reddy [18] have analyzed classical and nonclassical frequency ratios for

a Timoshenko microbeam. Demir et al. [19] have examined nonclassical frequencies of carbon nanotubes based on shear deformable beam theory by discrete singular convolution technique. Akgoz and Civalek [20] have analyzed microsized beams for various boundary conditions based on the strain gradient elasticity theory. In addition, small scale effect of the torsion response of bars and buckling of axially loaded microscaled beams has been presented by Kahrobaiyan et al. [21] and Akgoz and Civalek [22], respectively.

The objective of the present paper is to establish dynamic finite element model for microbeams of constant width and linearly varying depth by using both the basic equations of the strain gradient elasticity theory and weak form formulation of the dynamical equation. The material and microbeam models are assumed to obey the strain gradient theory, as developed by Papargyri-Beskou et al. [23]. In the first part of study, the basic equations of gradient elasticity theory are reviewed in Section 2. Then gradient elastic essential boundary conditions for static and dynamic analysis of microbeam obtained with the aid of weak form formulation of equation of motion. By using essential boundary conditions, interpolating functions are calculated for finite element procedure in Section 3. Section 4 is devoted to the construction of stiffness and mass matrix of the microbeam of constant width and linearly varying depth. Four representative numerical examples are solved and solutions are compared with their classical counterparts in Section 5. The paper gives a conclusion in Section 6.

2. Formulation of the Equation of Motion

2.1. Governing Equation for Bending. In the present study the following gradient elasticity theory is employed which is suitable for investigating the natural frequencies of microbeams [23]:

$$\sigma_{ij} = C_{ijkl}\left(\epsilon_{kl} - l^2\epsilon_{kl,mn}\right) \tag{1}$$

in which σ_{ij} and ϵ_{ij} represent the stress and strain tensors, C_{ijkl} represents the elastic moduli, and l denotes the simply gradient elastic modulus, representing the internal or characteristic length of the material microstructure. The kinetic and the potential energies of the microbeam shown in Figure 1 are then in the following form:

$$\begin{aligned} T &= \frac{1}{2}\rho\int_0^L A(x)\left(\frac{\partial v}{\partial t}\right)^2 dx, \\ U &= \frac{1}{2}E\int_0^L I(x)\left\{\left(\frac{\partial^2 v}{\partial x^2}\right)^2 - l^2\left(\frac{\partial^2 v}{\partial x^2}\frac{\partial^4 v}{\partial x^4}\right)\right\} dx, \end{aligned} \tag{2}$$

where ρ is the mass density, E is the modulus of elasticity, $I(x)$ is the moment of inertia about the axis x, and $A(x)$ is the cross sectional area. Note that $I(x)$, $A(x)$ quantities are variable. The variation of the external excitation force is obtained as

$$\delta W_E = \int_0^L F(x)\sin(\omega t)\,\delta v\,dx. \tag{3}$$

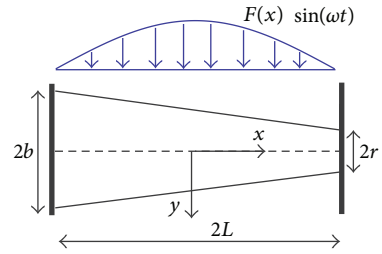

Figure 1: Schematic diagram of Cartesian coordinate system for a beam fixed at two ends.

In order to obtain the partial differential equation governing the motion of the system, above equations substituted into the Hamilton's principle resulting in

$$\begin{aligned} &\rho A(x)\frac{\partial^2 v}{\partial t^2} + EI(x)\left\{\left(\frac{\partial^4 v}{\partial x^4}\right) - l^2\left(\frac{\partial^6 v}{\partial x^6}\right)\right\} \\ &\quad -F(x)\sin(\omega t) = 0, \end{aligned} \tag{4}$$

with the following classical fixed boundary conditions for microbeam:

$$v|_{x=0} = v|_{x=L} = 0, \qquad \left.\frac{\partial v}{\partial x}\right|_{x=0} = \left.\frac{\partial v}{\partial x}\right|_{x=L} = 0. \tag{5}$$

It can be seen from (4) that the equation of motion of the microbeams is related to two parts: one associated with $\rho A(x)$ and $EI(x)$ as in classical microbeam model and the other associated with the material parameters $EI(x)l^2$.

3. Weak Form Formulation of the Equation of Motion and Discretization

In the gradient elastic finite element method, a variational description of the problem is needed first as in common finite element procedure [24]. The starting point for deriving the weak form is to multiply the partial differential equation of gradient elastic beam with a test function and integrate over the domain:

$$\begin{aligned} \int_0^L \psi(x)\Bigg(&\rho A\frac{\partial^2 v}{\partial t^2} + EI\left\{\left(\frac{\partial^4 v}{\partial x^4}\right) - l^2\left(\frac{\partial^6 v}{\partial x^6}\right)\right\} \\ &-F(x)\sin(\omega t)\Bigg)dx = 0, \end{aligned} \tag{6}$$

where $\psi(x)$ is the test function and integrating by parts

$$\begin{aligned} 0 = \int_0^L \Bigg(&EI\left[\frac{\partial^2\psi}{\partial x^2}\frac{\partial^2 v}{\partial x^2} - l^2\frac{\partial^3\psi}{\partial x^3}\frac{\partial^3 v}{\partial x^3}\right] \\ &-\psi(x)F(x)\sin(\omega t) + \psi(x)\rho A\frac{\partial^2 v}{\partial t^2}\Bigg)dx \end{aligned}$$

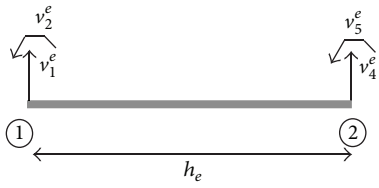

Figure 2: Two-node strain gradient microbeam element.

$$+\psi(x)\,EI\left\{\frac{\partial^3 v}{\partial x^3}-l^2\frac{\partial^5 v}{\partial x^5}\right\}_0^L - \frac{\partial\psi(x)}{\partial x}EI\left\{\frac{\partial^2 v}{\partial x^2}-l^2\frac{\partial^4 v}{\partial x^4}\right\}_0^L - l^2EI\left\{\frac{\partial^2\psi(x)}{\partial x^2}\frac{\partial^3\psi(x)}{\partial x^3}\right\}_0^L. \tag{7}$$

Presented equation (7) is a weak derivation of the equation of motion and the boundary conditions for the microbeams based on strain gradient elasticity theory and the Euler Bernoulli beam theory. From (7), gradient elastic essential boundary conditions for the microbeam clamped at two ends (see Figure 1) are

$$\begin{aligned} v|_{x=0} &= v|_{x=L} = 0,\\ \left.\frac{\partial v}{\partial x}\right|_{x=0} &= \left.\frac{\partial v}{\partial x}\right|_{x=L} = 0,\\ \left.\frac{\partial^3 v}{\partial^3 x}\right|_{x=0} &= \left.\frac{\partial^3 v}{\partial^3 x}\right|_{x=L} = 0. \end{aligned} \tag{8}$$

3.1. Interpolating Functions for Microbeams. In this section, the gradient elastic interpolating functions are calculated. The weak formulation of the equation of motion in (7) requires that the interpolation functions of one element should be continuous with nonzero derivatives up to three orders; then the essential boundary conditions in (8) are satisfied. The nodal degrees of freedom are indicated by the following expressions:

$$\begin{aligned} v_1^e &\equiv v(x_e) \qquad v_2^e \equiv \left(-\frac{dv}{dx}\right)\Big|_{x=x_e}\\ v_3^e &\equiv \left(-\frac{d^3v}{dx^3}\right)\Big|_{x=x_e} \qquad v_4^e \equiv v(x_{e+1})\\ v_5^e &\equiv \left(-\frac{dv}{dx}\right)\Big|_{x=x_{e+1}} \qquad v_6^e \equiv \left(-\frac{d^3v}{dx^3}\right)\Big|_{x=x_{e+1}}. \end{aligned} \tag{9}$$

Figure 2 shows two-node strain gradient microbeam element. It should be noted that v_3^e and v_6^e are strain gradient parameters, which is not shown in Figure 2. Since there is a total of six conditions in an element (three per node), a fifth degree polynomial can be selected for $v(x)$:

$$v(x) = \sum_{k=1}^{6} c_k x^{k-1}. \tag{10}$$

By using (9) and (10), nodal variables can be expressed in terms of c_i unknowns in the following compact form:

$$\begin{pmatrix} v_1^e\\ v_2^e\\ v_3^e\\ v_4^e\\ v_5^e\\ v_6^e \end{pmatrix} = \begin{pmatrix} 1 & x_e & x_e^2 & x_e^3 & x_e^4 & x_e^5\\ 0 & -1 & -2x_e & -3x_e^2 & -4x_e^3 & -5x_e^4\\ 0 & 0 & 0 & -6 & -24x_e & -60x_e^2\\ 1 & x_{e+1} & x_{e+1}^2 & x_{e+1}^3 & x_{e+1}^4 & x_{e+1}^5\\ 0 & -1 & -2x_{e+1} & -3x_{e+1}^2 & -4x_{e+1}^3 & -5x_{e+1}^4\\ 0 & 0 & 0 & -6 & -24x_{e+1} & -60x_{e+1}^2 \end{pmatrix} \times \begin{pmatrix} c_1\\ c_2\\ c_3\\ c_4\\ c_5\\ c_6 \end{pmatrix}. \tag{11}$$

Inverting this matrix equation to express c_i in terms of v_1^e, v_2^e, v_3^e, v_4^e, v_5^e, and v_6^e and substituting the result into (10), we obtain

$$v^e(x) = v_1^e\Omega_1^e + v_2^e\Omega_2^e + v_3^e\Omega_3^e + v_4^e\Omega_4^e + v_5^e\Omega_5^e + v_6^e\Omega_6^e = \sum_{j=1}^{6} v_j^e\Omega_j^e, \tag{12}$$

and the interpolation functions Ω_i^e in (12) can be expressed in terms of the local coordinate x:

$$\begin{aligned} \Omega_1^e(x) &= -\frac{x^5}{h_e^5}+\frac{5x^4}{2h_e^4}-\frac{5x^2}{2h_e^2}+1\\ \Omega_2^e(x) &= \frac{x^5}{2h_e^4}-\frac{5x^4}{4h_e^3}+\frac{7x^2}{4h_e}-x\\ \Omega_3^e(x) &= -\frac{x^5}{24h_e^2}+\frac{7x^4}{48h_e}+\frac{x^2h_e}{16}-\frac{x^3}{6}\\ \Omega_4^e(x) &= \frac{x^5}{h_e^5}-\frac{5x^4}{2h_e^4}+\frac{5x^2}{2h_e^2}\\ \Omega_5^e(x) &= \frac{x^5}{2h_e^4}-\frac{5x^4}{4h_e^3}+\frac{3x^2}{4h_e}\\ \Omega_6^e(x) &= -\frac{x^5}{24h_e^2}+\frac{x^4}{16h_e}-\frac{x^2h_e}{48}, \end{aligned} \tag{13}$$

where $x_{e+1} = x_e + h_e$ and h_e is the length of element.

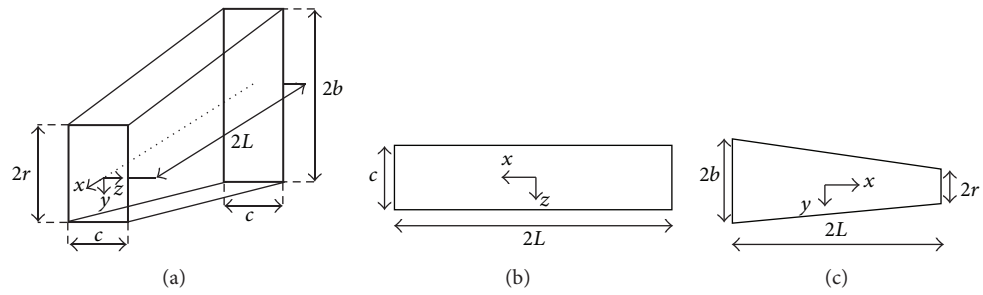

Figure 3: Geometry of a constant width and linearly varying depth microbeam.

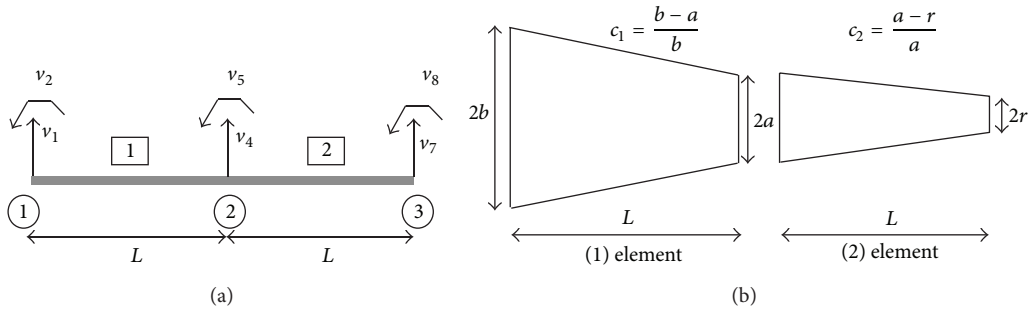

Figure 4: Finite element discretization of the microbeam.

4. Construction of Gradient Elastic Stiffness and Mass Matrices

4.1. Developing the Strain Gradient Microbeam Finite Element Model. In this section the stiffness and mass matrix of a strain gradient microbeam element developed and during an example. The total length of the microbeam is $2L$, as seen in Figure 3. It has nonuniform cross section $I(x)$. The modulus of elasticity E is taken as a constant for each element. The microbeam is fixed at two points such that the problem is statically indeterminate. In order to compute the free vibration frequencies, the external excitation force is taken as zero in (6). To illustrate the use of finite elements for gradient elastic microbeams discretized the beam longitudinally with two beam elements, as seen in Figure 4. Considering a section at a distance x from fixed end, as shown in the Figure 1. The variation of the $I_1(x)$ and $A_1(x)$ over the first element is as follows:

$$I_1(x) = \frac{2}{3}b^3c\left[1 - \frac{c_1 x}{L}\right]^3$$
$$A_1(x) = 2bc\left[1 - \frac{c_1 x}{L}\right] \tag{14}$$
$$c_1 = \frac{b-a}{b}.$$

Similarly, the moment of inertia and area of the second element with respect to x axis are

$$I_2(x) = \frac{2}{3}a^3c\left[1 - \frac{c_2 x}{L}\right]^3$$
$$A_2(x) = 2ac\left[1 - \frac{c_2 x}{L}\right]$$
$$c_2 = \frac{a-r}{a}. \tag{15}$$

4.2. Gradient Elastic Stiffness and Mass Matrices. The gradient elastic finite element model is obtained as in common classical finite element procedure by substituting interpolation functions into the weak form formulation of (6) which leads to the following equations:

$$K_{ij}^e = \int_{x_e}^{x_{e+1}} \left\{ EI(x) \left[\frac{\partial^2 \Omega_i(x)}{\partial x^2} \frac{\partial^2 \Omega_j(x)}{\partial x^2} - l^2 \frac{\partial^3 \Omega_i(x)}{\partial x^3} \frac{\partial^3 \Omega_j(x)}{\partial x^3} \right] \right\} dx \tag{16}$$

$$M_{ij}^e = \int_{x_e}^{x_{e+1}} \left\{ \rho A(x) \left(\Omega_i(x)\, \Omega_j(x) \right) \right\} dx, \tag{17}$$

where $\Omega_i(x)$, $\Omega_j(x)$ are interpolating functions ($i, j = 1, 2, 3, 4, 5, 6$) and the stiffness $[K]$ and mass $[M]$ matrices are expressed as follows:

$$[K^e] = \begin{pmatrix} k_{11} & k_{12} & k_{13} & k_{14} & k_{15} & k_{16} \\ & k_{22} & k_{23} & k_{24} & k_{25} & k_{26} \\ & & k_{33} & k_{34} & k_{35} & k_{36} \\ & & & k_{44} & k_{45} & k_{46} \\ & \text{sym} & & & k_{55} & k_{56} \\ & & & & & k_{66} \end{pmatrix};$$

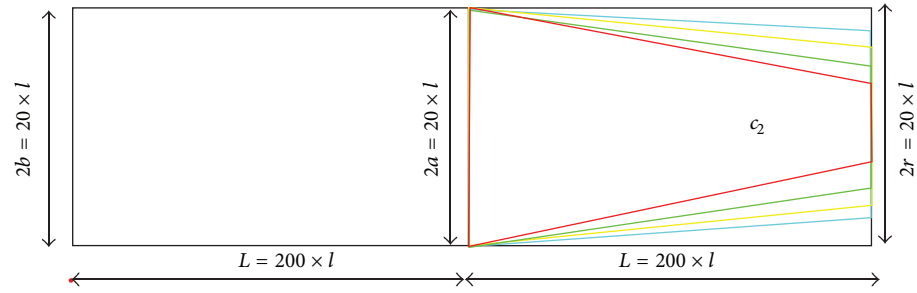

FIGURE 5: Schematic diagram for the variation of c_2 and r.

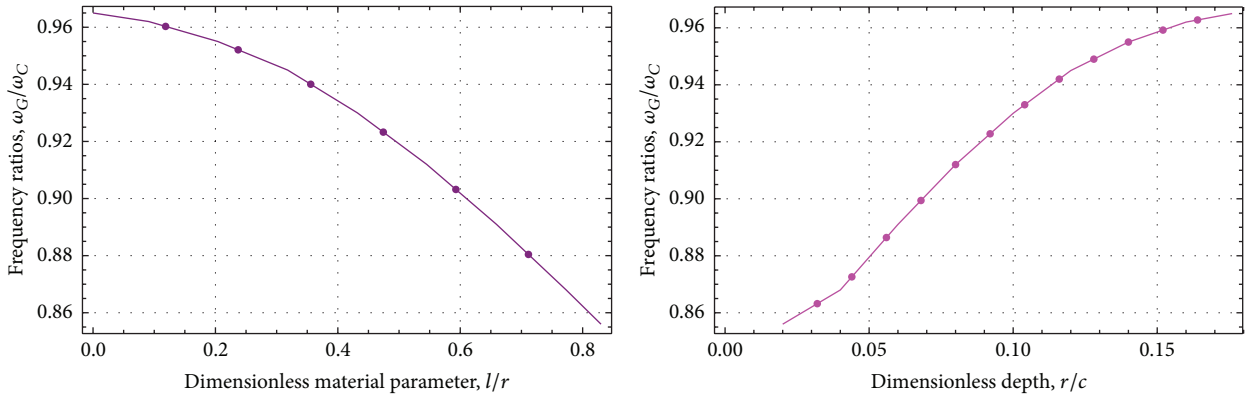

FIGURE 6: Effect of the dimensionless material parameter and dimensionless depth on the frequency ratio for $L/l = 200$, $b/l = a/l = 10$, and $c = 1\,\mu$m.

$$[M^e] = \begin{pmatrix} m_{11} & m_{12} & m_{13} & m_{14} & m_{15} & m_{16} \\ & m_{22} & m_{23} & m_{24} & m_{25} & m_{26} \\ & & m_{33} & m_{34} & m_{35} & m_{36} \\ & & & m_{44} & m_{45} & m_{46} \\ & \text{sym} & & & m_{55} & m_{56} \\ & & & & & m_{66} \end{pmatrix}, \tag{18}$$

where "sym" refers to the symmetric nature of the stiffness and mass matrices. The stiffness matrix for the first element is computed with the aid of (16):

$$k_{11}^{(1)} = E\left(-\frac{335b^3cc_1^3}{126L^3} + \frac{590b^3cc_1^2}{63L^3} - \frac{85b^3cc_1}{7L^3} + \frac{170b^3c}{21L^3} - \frac{120l^2}{L^5}\right)$$

$$k_{12}^{(1)} = E\left(\frac{b^3c\left(185c_1^3 - 676c_1^2 + 1026c_1 - 1020\right)}{252L^2} + \frac{60l^2}{L^4}\right)$$

$$k_{13}^{(1)} = -\frac{b^3Ec\left(51c_1^3 - 172c_1^2 + 198c_1 - 12\right)}{3024}$$

$$k_{14}^{(1)} = E\left(\frac{335b^3cc_1^3}{126L^3} - \frac{590b^3cc_1^2}{63L^3} + \frac{85b^3cc_1}{7L^3} - \frac{170b^3c}{21L^3} + \frac{120l^2}{L^5}\right)$$

$$k_{15}^{(1)} = E\left(\frac{b^3c\left(485c_1^3 - 1684c_1^2 + 2034c_1 - 1020\right)}{252L^2} + \frac{60l^2}{L^4}\right)$$

$$k_{16}^{(1)} = \frac{b^3Ec\left(65c_1^3 - 188c_1^2 + 162c_1 + 12\right)}{3024}$$

$$k_{22}^{(1)} = E\left(\frac{b^3c\left(-119c_1^3 + 508c_1^2 - 1026c_1 + 1356\right)}{504L} - \frac{30l^2}{L^3}\right)$$

$$k_{23}^{(1)} = \frac{b^3Ec\left(177c_1^3 - 692c_1^2 + 990c_1 - 60\right)L}{30240}$$

$$k_{24}^{(1)} = E\left(\frac{b^3c\left(-185c_1^3 + 676c_1^2 - 1026c_1 + 1020\right)}{252L^2} - \frac{60l^2}{L^4}\right)$$

$$k_{25}^{(1)} = E\left(-\frac{b^3c\left(c_1 - 2\right)\left(c_1\left(251c_1 - 342\right) + 342\right)}{504L} - \frac{30l^2}{L^3}\right)$$

$$k_{26}^{(1)} = \frac{b^3Ec\left(235c_1^3 - 772c_1^2 + 810c_1 + 60\right)L}{30240}$$

$$k_{33}^{(1)} = E\left(\frac{b^3c\left(c_1\left(-59\left(c_1 - 4\right)c_1 - 378\right) + 396\right)L^3}{362880} - \frac{l^2L}{8}\right)$$

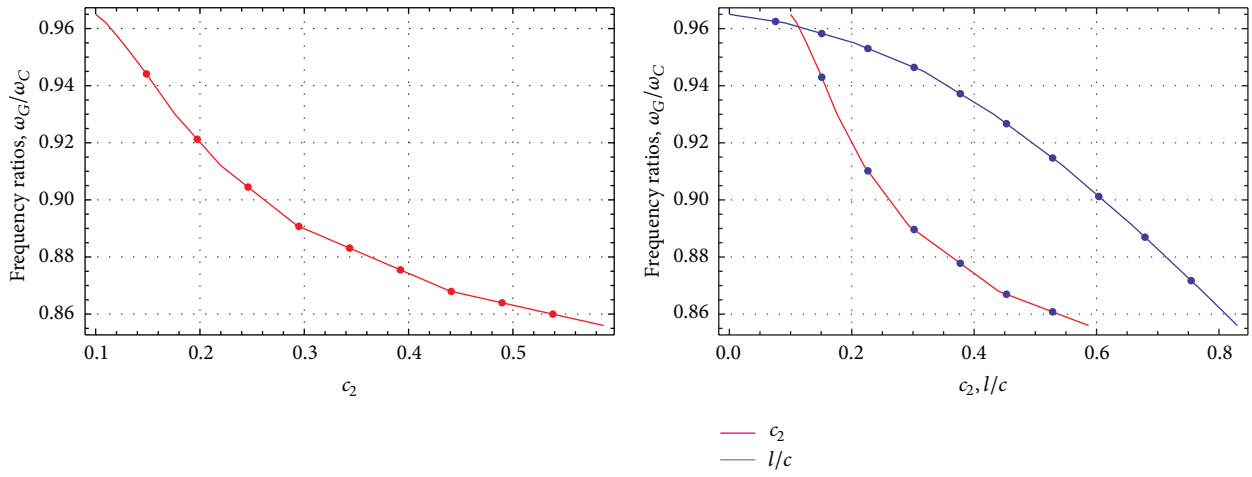

FIGURE 7: Effect of the dimensionless material parameter and slope of second element c_2 on the frequency ratio for $L/l = 200$, $b/l = a/l = 10$, and $c = 1$ mm.

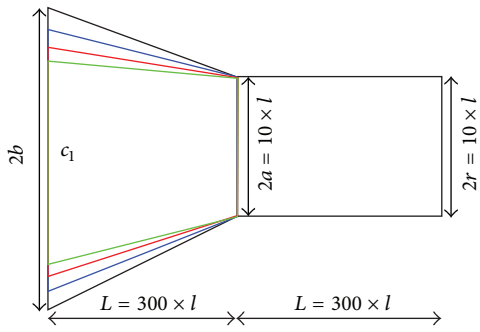

FIGURE 8: Schematic diagram for the variation of c_1 and b.

$$k_{34}^{(1)} = \frac{b^3 Ec\left(51c_1^3 - 172c_1^2 + 198c_1 - 12\right)}{3024}$$

$$k_{35}^{(1)} = \frac{b^3 Ec\left(333c_1^3 - 1028c_1^2 + 990c_1 - 60\right)L}{30240}$$

$$k_{36}^{(1)} = E\left(\frac{b^3 c\left(c_1 - 2\right)\left(c_1\left(89c_1 - 138\right) + 138\right)L^3}{362880} + \frac{l^2 L}{24}\right)$$

$$k_{44}^{(1)} = E\left(-\frac{335b^3 cc_1^3}{126L^3} + \frac{590b^3 cc_1^2}{63L^3} - \frac{85b^3 cc_1}{7L^3} + \frac{170b^3 c}{21L^3} - \frac{120l^2}{L^5}\right)$$

$$k_{45}^{(1)} = E\left(\frac{b^3 c\left(-485c_1^3 + 1684c_1^2 - 2034c_1 + 1020\right)}{252L^2} - \frac{60l^2}{L^4}\right)$$

$$k_{46}^{(1)} = -\frac{b^3 Ec\left(65c_1^3 - 188c_1^2 + 162c_1 + 12\right)}{3024}$$

$$k_{55}^{(1)} = E\left(\frac{b^3 c\left(-719c_1^3 + 2524c_1^2 - 3042c_1 + 1356\right)}{504L} - \frac{30l^2}{L^3}\right)$$

$$k_{56}^{(1)} = -\frac{b^3 Ec\left(415c_1^3 - 1108c_1^2 + 810c_1 + 60\right)L}{30240}$$

$$k_{66}^{(1)} = E\left(\frac{b^3 c\left(-195c_1^3 + 668c_1^2 - 810c_1 + 396\right)L^3}{362880} - \frac{l^2 L}{8}\right). \quad (19)$$

By using (17), the elements of mass matrix for the first element can be written as follows:

$$m_{11}^{(1)} = \rho\left(\frac{2077bcL}{2772} - \frac{955bcc_1 L}{5544}\right)$$

$$m_{12}^{(1)} = \rho\left(\frac{31}{924}bcc_1 L^2 - \frac{74}{693}bcL^2\right)$$

$$m_{13}^{(1)} = \rho\left(\frac{169bcL^4}{110880} - \frac{2bcc_1 L^4}{3465}\right)$$

$$m_{14}^{(1)} = \rho\left(\frac{695bcL}{2772} - \frac{695bcc_1 L}{5544}\right)$$

$$m_{15}^{(1)} = \rho\left(\frac{83bcL^2}{1386} - \frac{155bcc_1 L^2}{5544}\right)$$

$$m_{16}^{(1)} = \rho\left(\frac{bcc_1 L^4}{1848} - \frac{139bcL^4}{110880}\right)$$

$$m_{22}^{(1)} = \rho\left(\frac{1079bcL^3}{55440} - \frac{793bcc_1 L^3}{110880}\right)$$

$$m_{23}^{(1)} = \rho\left(\frac{5bcc_1 L^5}{38016} - \frac{bcL^5}{3168}\right)$$

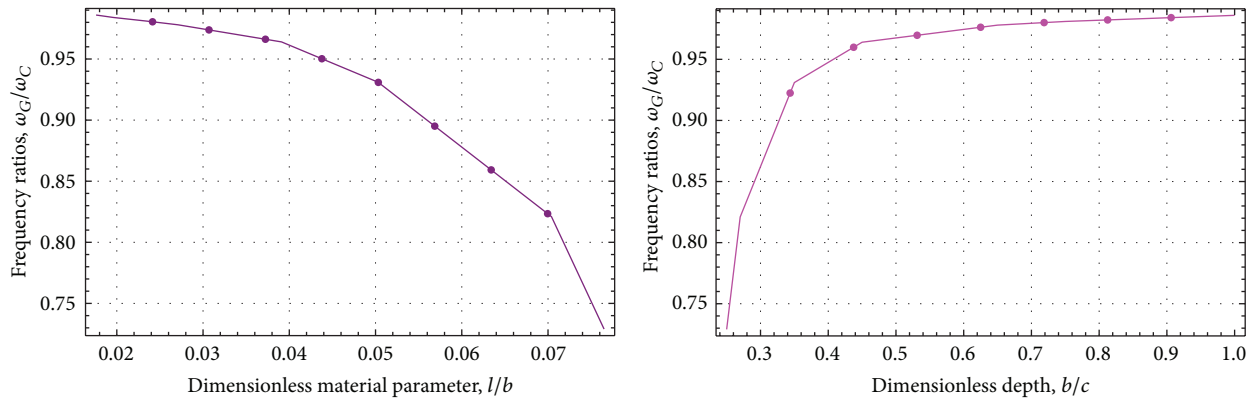

(a) (b)

FIGURE 9: Effect of the dimensionless material parameter and dimensionless depth on the frequency ratio for $L/l = 200$, $b/l = a/l = 10$, and $c = 1$ mm.

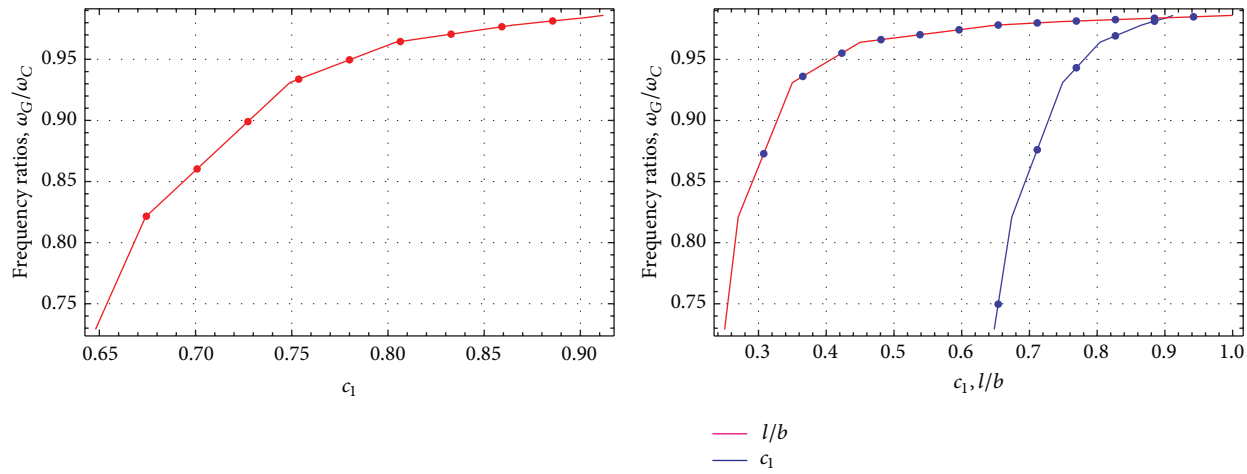

(a) (b)

FIGURE 10: Effect of the dimensionless material parameter and slope of first element c_1 on the frequency ratio for $L/l = 300$, $a/l = r/l = 5$, and $c = 1$ mm.

$$
\begin{aligned}
m_{24}^{(1)} &= \rho\left(\frac{59bcc_1L^2}{1848} - \frac{83bcL^2}{1386}\right)\\
m_{25}^{(1)} &= \rho\left(\frac{769bcc_1L^3}{110880} - \frac{769bcL^3}{55440}\right)\\
m_{26}^{(1)} &= \rho\left(\frac{31bcL^5}{110880} - \frac{173bcc_1L^5}{1330560}\right)\\
m_{33}^{(1)} &= \rho\left(\frac{bcL^7}{177408} - \frac{41bcc_1L^7}{15966720}\right)\\
m_{34}^{(1)} &= \rho\left(\frac{139bcL^4}{110880} - \frac{79bcc_1L^4}{110880}\right)\\
m_{35}^{(1)} &= \rho\left(\frac{31bcL^5}{110880} - \frac{199bcc_1L^5}{1330560}\right)\\
m_{36}^{(1)} &= \rho\left(\frac{43bcc_1L^7}{15966720} - \frac{43bcL^7}{7983360}\right)\\
m_{44}^{(1)} &= \rho\left(\frac{2077bcL}{2772} - \frac{457}{792}bcc_1L\right)\\
m_{45}^{(1)} &= \rho\left(\frac{74}{693}bcL^2 - \frac{29}{396}bcc_1L^2\right)\\
m_{46}^{(1)} &= \rho\left(\frac{bcc_1L^4}{1056} - \frac{169bcL^4}{110880}\right)\\
m_{55}^{(1)} &= \rho\left(\frac{1079bcL^3}{55440} - \frac{13bcc_1L^3}{1056}\right)\\
m_{56}^{(1)} &= \rho\left(\frac{7bcc_1L^5}{38016} - \frac{bcL^5}{3168}\right)\\
m_{66}^{(1)} &= \rho\left(\frac{bcL^7}{177408} - \frac{7bcc_1L^7}{2280960}\right).
\end{aligned}
\tag{20}
$$

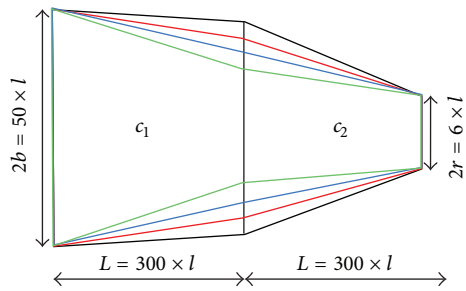

Figure 11: Schematic diagram for the variation of c_1 and c_2.

Similarly, the mass and the stiffness matrices of the second element can be calculated by replacing (c_1) by (c_2) and (b) by (a). Inserting above equations in (18) leads to following eigenvalue problem:

$$\left\{[K] - \omega^2 [M]\right\} [\Delta] = 0, \tag{21}$$

where $[K]$ is the stiffness matrix with respect to the local coordinates, $[M]$ is the mass matrix, $[\Delta]$ is column vector of unknown coefficients, and ω is free vibration frequencies. It is noted that during the assembly of the matrices, the components of the natural boundary condition vector will be cancelled. For a nontrivial solution, determinant of the assembled coefficient matrix must be zero as follows:

$$\text{Det}\left\{\begin{pmatrix} \widetilde{K}_{11} & \widetilde{K}_{12} & \widetilde{K}_{13} \\ \widetilde{K}_{21} & \widetilde{K}_{22} & \widetilde{K}_{23} \\ \widetilde{K}_{31} & \widetilde{K}_{32} & \widetilde{K}_{33} \end{pmatrix} - \omega^2 \begin{pmatrix} \widetilde{M}_{11} & \widetilde{M}_{12} & \widetilde{M}_{13} \\ \widetilde{M}_{21} & \widetilde{M}_{22} & \widetilde{M}_{23} \\ \widetilde{M}_{31} & \widetilde{M}_{32} & \widetilde{M}_{33} \end{pmatrix}\right\} = 0. \tag{22}$$

It should be noted that the dimension of the assembled matrix in (22) is 3×3 while, in classical elasticity, the dimension of the assembled matrix is 2×2. The advantage of this determinant is capability of considering any possible combination of slopes. The problem is an eigenvalue problem and determinant of coefficient matrix yields a characteristic equation and the roots of the characteristic equation give the natural frequencies for the microbeam with varying cross section.

5. Results for the Natural Frequencies

In this section, four numerical examples are presented and discussed to verify the accuracy of the present finite element model based on gradient elasticity. The microbeam considered here is steel ($E = 210\,\text{GPa}$, $\rho = 8166\,\text{kg/m}^3$). It should be noted that the material scale parameter is taken as ($\gamma = 17.6\,\mu\text{m}$) for homogeneous epoxy beam [8].

5.1. Effect of the Material Length Scale Parameter and Slope of Second Element. In order to see the effect of (c_2) on the first natural frequency, the gradient elasticity and classical elasticity frequency ratios are presented for various slope values. The dimensionless material length scale parameter is considered as $(l/r = 0.1, \ldots, 0.8)$. For illustration purpose, the following parameters are used in calculating the numerical results: ($L = 200l$, $c = 1\,\text{mm}$, and $b = a = 10l$). Figure 5 shows the variation of slope (c_2) schematically; Figure 6 contains plots of the dimensionless depth (r/c) and material parameter (l/r) versus first frequency ratios (classical and gradient theories). As expected, the strain gradient effects are significant when (l/r) ratio is high. In Figure 7 for various values of (l/r) are assessed. In other words, last point thickness of the microbeam (r) is varied when the other thicknesses are keep constant as $(b = a = 10l)$. It is clearly seen that the last point thickness decreases as the dimensionless material scale parameter (l/r) increases. When the dimensionless material parameter (l/r) and the slope of second element (c_2) increase, the first frequency ratios decrease and the difference between the two models is significant, as seen from Figure 7. It is shown that the difference among the predicted frequency values is diminishing when the thickness of the microbeam becomes larger, thereby indicating that the small size effect is only significant when the thickness of the microbeam is comparable to the material length scale parameter. From the results, the reason of differences between the frequencies predicted by two theories can be simply explained by the material length scale parameter in the constitutive equation.

5.2. Effect of the Material Length Scale Parameter and Slope of First Element. In the second example, first frequency ratios are examined for various values of the slope (c_1). The dimensionless material length scale parameters are taken as $(l/b = 0.01, \ldots, 0.08)$. The following parameters are used in computing the numerical solutions: ($L = 300l$, $c = 1\,\text{mm}$, and $r = a = 5l$). Figure 8 shows the variation of slope (c_1) schematically. The effects of c_1 and dimensionless material length scale parameter on the first frequency ratio are demonstrated in Figures 9 and 10. Figure 9 contains plots of the dimensionless depth (b/c) and material parameter (l/b) versus frequency ratios (classical and gradient theories). It is interesting to note that as the dimensionless material parameter (l/b) and the slope of first element (c_1) increase, the frequency ratios also increases, as seen from Figure 10.

5.3. Effect of the Material Length Scale Parameter and Slopes. This subsection deals with the effect of slopes and slope ratios on the free vibration frequencies of a microbeam. The following parameters are used in this example: ($L = 300l$, $c = 1\,\text{mm}$), and the difference between the two models is examined. In this example, the microbeam midpoint thickness (a) is varied when both first and last point depth are keep constant as ($b = 25l$, $r = 3l$). Namely, the slope of first element (c_1) increases, when the slope of second element (c_2) decreases. Figure 11 shows the variation of c_1 and c_2. The effects of midpoint depth, slopes (c_1, c_2), and slope ratios $(c_1/c_2, c_2/c_1)$ on the frequency ratios are demonstrated in Figures 12 and 13. It can be concluded that the slopes (c_1, c_2) play the essential role in increasing or decreasing the first natural frequency for the microbeam. Also, it can be inferred that the frequencies of microbeam can be controlled by choosing proper values of (c_1) and (c_2), as seen from Figure 13. However, the small size effects are almost diminishing as

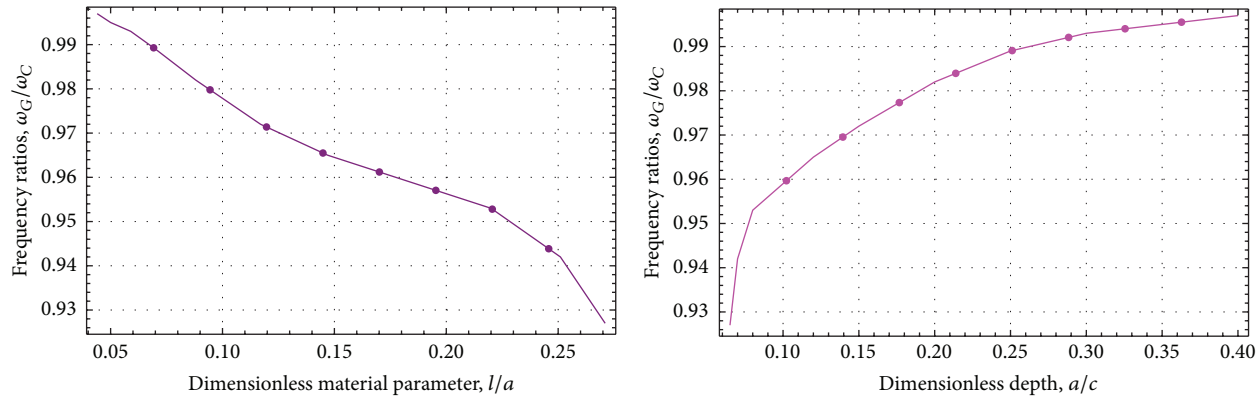

FIGURE 12: Effect of the dimensionless material parameter and dimensionless depth on the frequency ratio for $L/l = 200$, $b/l = a/l = 10$, and $c = 1\ \mu$m.

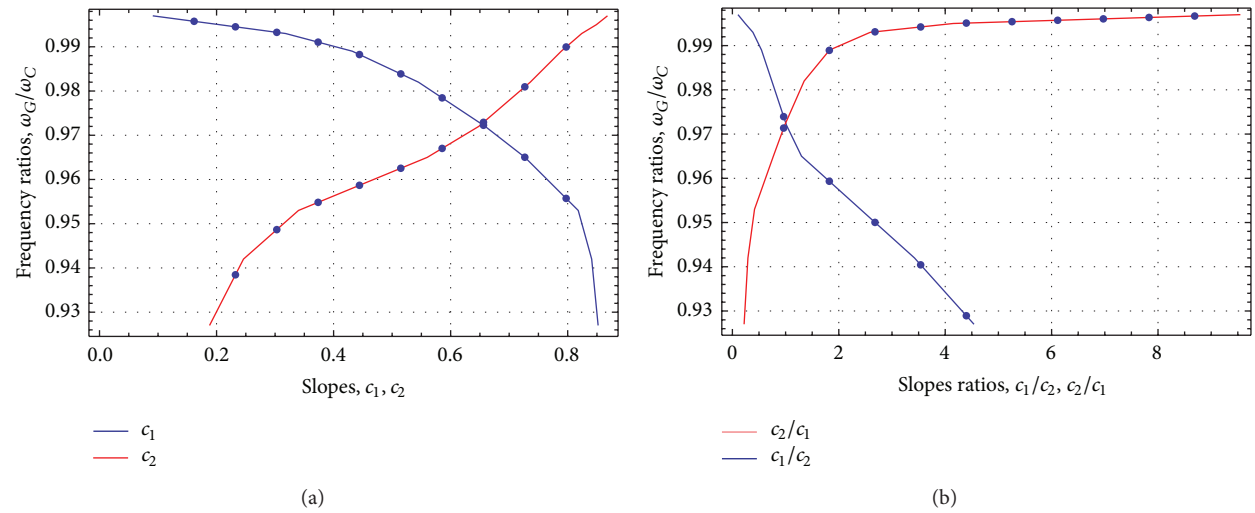

FIGURE 13: Effect of the slopes and slope ratios c_1, c_2, c_1/c_2, and c_2/c_1 on the frequency ratio for $L/l = 300$, $b/l = 25$, $r/l = 3$, and $c = 1$ mm.

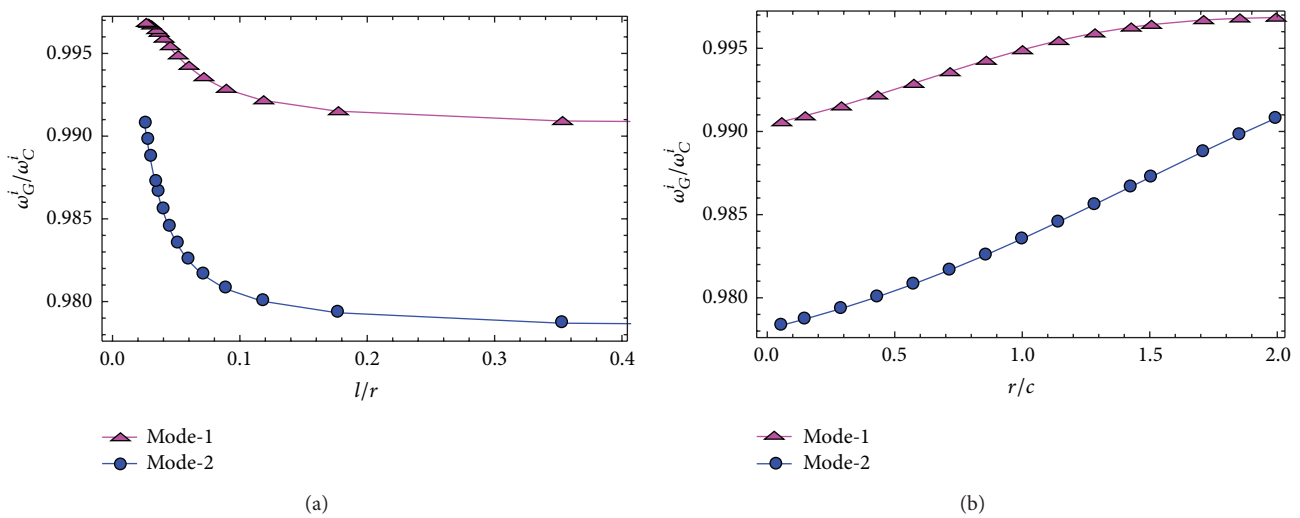

FIGURE 14: Effect of the dimensionless material parameter on the first two frequencies for $L/l = 200$, $b/l = a/l = 30$, and $c/l = 20$.

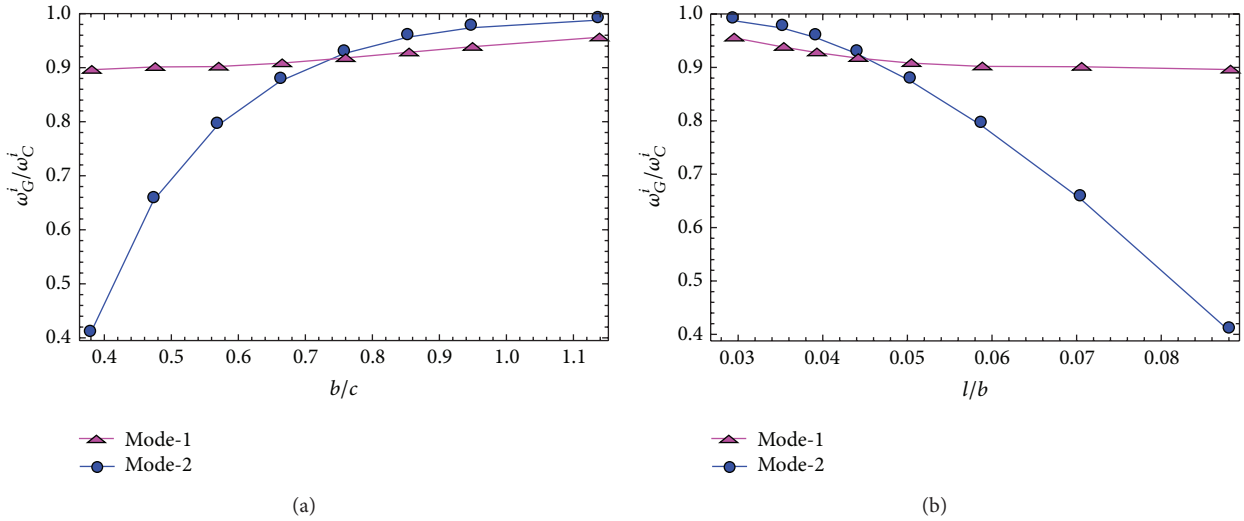

FIGURE 15: Effect of the dimensionless material parameter on the first two frequencies for $L/l = 200$, $r/l = a/l = 10$, and $c/l = 30$.

the depths of the microbeam is far greater than the material length scale parameter.

5.4. Effect of the Material Length Scale Parameter on the Second Mode. To investigate the effects of the length scale parameter on the first two frequencies of microbeam, frequency ratios are plotted in Figures 14-15 for various values of length scale parameter. According to these figures the first two frequency ratios are less than unity. It can be concluded from the figures that the effect of the length scale parameter on Mode-2 is more than on Mode-1. The difference between gradient and classical elasticity results for vibration frequencies is changing with slopes and material scale parameter.

6. Conclusion

In this study, an analysis has been performed for the evaluation of the natural frequencies of microbeams of constant width and linearly varying depth. The equation of motion and boundary conditions are obtained by a combination of the weak formulation and the basic equations of gradient elasticity. A finite element formulation is proposed for computation of natural frequencies and its numerical implementation is then verified obtaining a good agreement with classical data available in the scientific literature. Four numerical examples are solved and the small size effects on the natural frequencies are assessed for various slope values. Numerical results are presented in a series of figures to examine the effect of material parameter on the natural frequencies. The results reveal that for the microbeam with varying cross section comparable to its material length scale parameter, the effect of strain gradient is significant. As expected, it is also found that the present model exhibit size dependence when the depth of the microbeam approaches the material scale parameter. In addition the slopes have a great influence on the dynamic behavior of microbeam. It can be concluded that the frequencies of microbeam can be controlled by choosing proper values of depths. The present solution is very useful to analyze microbeams with linear varying cross section.

Conflict of Interests

The author declares that there is no conflict of interests regarding the publication of this paper.

References

[1] E. S. Hung and S. D. Senturia, "Extending the travel range of analog-tuned electrostatic actuators," *Journal of Microelectromechanical Systems*, vol. 8, no. 4, pp. 497–505, 1999.

[2] P. Attia, G. Tremblay, R. Laval, and P. Hesto, "Characterisation of a low-voltage actuated gold microswitch," *Materials Science and Engineering B*, vol. 51, no. 1–3, pp. 263–266, 1998.

[3] H. A. C. Tilmans and R. Legtenberg, "Electrostatically driven vacuum-encapsulated polysilicon resonators—part II: theory and performance," *Sensors and Actuators A*, vol. 45, no. 1, pp. 67–84, 1994.

[4] M. H. Kahrobaiyan, M. T. Ahmadian, P. Haghighi, and A. Haghighi, "Sensitivity and resonant frequency of an AFM with sidewall and top-surface probes for both flexural and torsional modes," *International Journal of Mechanical Sciences*, vol. 52, no. 10, pp. 1357–1365, 2010.

[5] Y. Moser and M. A. M. Gijs, "Miniaturized flexible temperature sensor," *Journal of Microelectromechanical Systems*, vol. 16, no. 6, pp. 1349–1354, 2007.

[6] A. W. Mcfarland and J. S. Colton, "Role of material microstructure in plate stiffness with relevance to microcantilever sensors," *Journal of Micromechanics and Microengineering*, vol. 15, no. 5, pp. 1060–1067, 2005.

[7] N. A. Fleck, G. M. Muller, M. F. Ashby, and J. W. Hutchinson, "Strain gradient plasticity: theory and experiment," *Acta Metallurgica et Materialia*, vol. 42, no. 2, pp. 475–487, 1994.

[8] D. C. C. Lam, F. Yang, A. C. M. Chong, J. Wang, and P. Tong, "Experiments and theory in strain gradient elasticity," *Journal of the Mechanics and Physics of Solids*, vol. 51, no. 8, pp. 1477–1508, 2003.

[9] J. S. Stolken and A. G. Evans, "Microbend test method for measuring the plasticity length scale," *Acta Materialia*, vol. 46, no. 14, pp. 5109–5115, 1998.

[10] R. D. Mindlin, "Micro-structure in linear elasticity," *Archive for Rational Mechanics and Analysis*, vol. 16, no. 1, pp. 51–78, 1964.

[11] R. A. Toupin, "Elastic materials with couple-stresses," *Archive for Rational Mechanics and Analysis*, vol. 11, no. 1, pp. 385–414, 1962.

[12] S. J. Zhou and Z. Q. Li, "Length scales in the static and dynamic torsion of a circular cylindrical micro-bar," *Journal of Shandong University of Technology*, vol. 31, no. 5, pp. 401–407, 2001.

[13] X. Kang and Z. Xi, "Size effect on the dynamic characteristic of a micro beam based on Cosserat theory," *Journal of Mechanical Strength*, vol. 29, no. 1, pp. 1–4, 2007.

[14] R. D. Mindlin, "Second gradient of strain and surface-tension in linear elasticity," *International Journal of Solids and Structures*, vol. 1, no. 4, pp. 417–438, 1965.

[15] S. K. Park and X. L. Gao, "Bernoulli-Euler beam model based on a modified couple stress theory," *Journal of Micromechanics and Microengineering*, vol. 16, no. 11, pp. 2355–2359, 2006.

[16] S. L. Kong, S. J. Zhou, Z. F. Nie, and K. Wang, "The size-dependent natural frequency of Bernoulli-Euler micro-beams," *International Journal of Engineering Science*, vol. 46, no. 5, pp. 427–437, 2008.

[17] H. M. Ma, X. L. Gao, and J. N. Reddy, "A microstructure-dependent Timoshenko beam model based on a modified couple stress theory," *Journal of the Mechanics and Physics of Solids*, vol. 56, no. 12, pp. 3379–3391, 2008.

[18] J. V. A. dos Santos and J. N. Reddy, "Vibration of Timoshenko beams using non-classical elasticity theories," *Shock and Vibration*, vol. 19, no. 3, pp. 251–256, 2011.

[19] C. Demir, O. Civalek, and B. Akgoz, "Free vibration analysis of carbon nanotubes based on shear deformable beam theory by discrete singular convolution technique," *Mathematical and Computational Applications*, vol. 15, no. 1, pp. 57–65, 2010.

[20] B. Akgoz and O. Civalek, "Analysis of micro-sized beams for various boundary conditions based on the strain gradient elasticity theory," *Archive of Applied Mechanics*, vol. 82, no. 3, pp. 423–443, 2012.

[21] M. H. Kahrobaiyan, S. A. Tajalli, M. R. Movahhedy, J. Akbari, and M. T. Ahmadian, "Torsion of strain gradient bars," *International Journal of Engineering Science*, vol. 49, no. 9, pp. 856–866, 2011.

[22] B. Akgoz and O. Civalek, "Strain gradient elasticity and modified couple stress models for buckling analysis of axially loaded micro-scaled beams," *International Journal of Engineering Science*, vol. 49, no. 11, pp. 1268–1280, 2011.

[23] S. Papargyri-Beskou, K. G. Tsepoura, D. Polyzos, and D. E. Beskos, "Bending and stability analysis of gradient elastic beams," *International Journal of Solids and Structures*, vol. 40, no. 2, pp. 385–400, 2003.

[24] M. O. Yayli, "Weak formulation of finite element method for nonlocal beams using additional boundary conditions," *Journal of Computational and Theoretical Nanoscience*, vol. 8, no. 11, pp. 2173–2180, 2011.